Inorg. Chem. **2006**, *45*, 3399–3407

The Electronic Ground State of $[V(urea)_6]^{3+}$ Probed by NIR Luminescence, Electronic Raman, and High-Field EPR Spectroscopies

Rémi Beaulac,[†] Philip L. W. Tregenna-Piggott,[‡] Anne-Laure Barra,[§] Høgni Weihe,[||] Dominique Luneau,[⊥] and Christian Reber*[,†]

Département de Chimie, Université de Montréal, Montréal, Québec, Canada, Laboratory for Neutron Scattering, ETHZ and Paul-Scherrer Institute, Villigen, Switzerland, Grenoble High Magnetic Field Laboratory, Grenoble, France, Department of Chemistry, University of Copenhagen, Copenhagen, Denmark, and Cristallographie et Ingénierie Moléculaire, Laboratoire des Multimatériaux et Interfaces (UMR 5615), Université Claude-Bernard Lyon 1, Villeurbanne, France

Received October 4, 2005

The electronic structure of a trigonally distorted vanadium(III) complex, $[V(urea)_6](ClO_4)_3$, and its deuterated analogue, $[V(urea\text{-}d_4)_6](ClO_4)_3$ has been investigated with Raman, luminescence, and high-frequency high-field electron paramagnetic resonance spectroscopies and with magnetic measurements. A broad electronic Raman transition is observed at around 1400 cm^{-1} and attributed to a transition to the ^3E (D_3) component of the $^3T_{1g}$ (O_h) ground state. The same splitting is seen in the near-infrared luminescence spectrum in the form of a similarly broad peak at 8450 cm^{-1}, 1400 cm^{-1} lower in energy than the $^1E \rightarrow {}^3A_2$ spin-flip transition. Powder high-frequency and high-field electron paramagnetic resonance spectra, magnetic susceptibilities, and magnetization studies give a precise measurement of the zero-field splitting and of the g values in this complex ($D = 6.00(2)$ cm^{-1}, $E = 0.573(6)$ cm^{-1}, $g_x = 1.848(2)$, $g_y = 1.832(4)$, and $g_z = 1.946(7)$). A set of angular overlap model parameters is proposed that reproduces all spectroscopic observations, and an analysis of the influence of the bonding of urea on the trigonal distortion of the complex is given.

1. Introduction

The electronic structure of octahedral coordination compounds containing transition-metal ions with the d^2 configuration is a classic case used to present ligand-field theory[1−4] and has been probed for more than 50 years with a variety of experimental techniques.[5−12] One area of current interest is the use of these complexes for near-infrared (NIR) to visible upconversion of light,[13] illustrating the need for a detailed determination of their electronic structure, an aspect of key importance for understanding these phenomena. The characterization of low-lying electronic states of many transition metal complexes is challenging, from both experimental[14−18] and theoretical[19−24] perspectives. This challenge is illustrated by the study of deceptively simple

* To whom correspondence should be addressed. E-mail: reber@chimie.umontreal.ca. Tel.: (514) 343−7332. Fax: (514) 343−7586.
[†] Université de Montréal.
[‡] ETHZ and Paul-Scherrer Institute.
[§] Grenoble High Magnetic Field Laboratory.
[||] University of Copenhagen.
[⊥] Université Claude-Bernard Lyon 1.

(1) Bethe, H. *Ann. Phys. (Berlin)* **1929**, *3*, 133−208.
(2) Griffith, J. S. *The Theory of Transition-Metal Ions;* Cambridge University Press: Cambridge, U.K., 1961.
(3) Ballhausen, C. J. *Introduction to Ligand-Field Theory;* McGraw-Hill: New York, 1962.
(4) Liehr, A. D.; Ballhausen, C. J. *Ann. Phys. (Orlando, FL, U.S.)* **1959**, *2*, 134−155.
(5) Van Vleck, J. H. *J. Chem. Phys.* **1939**, *7*, 61−71.
(6) Ballhausen, C. J.; Winther, F. *Acta Chem. Scand.* **1959**, *13*, 1729−1732.
(7) Bennett, R. M.; Holmes, O. G. *Can. J. Chem.* **1960**, *38*, 2319−2323.
(8) Figgis, B. N.; Lewis, J.; Mabbs, F. *J. Chem. Soc.* **1960**, 2480−2485.
(9) Pryce, M. L. H.; Runciman, W. A. *Discuss. Faraday Soc.* **1958**, *26*, 34−42.
(10) Macfarlane, R. M. *J. Chem. Phys.* **1964**, *40*, 373−377.
(11) Machin, D. J.; Murray, K. S. *J. Chem. Soc. A* **1967**, *9*, 1498−1504.
(12) Casey, A. T.; Clark, R. J. H. *Inorg. Chem.* **1968**, *7*, 1598−1602.
(13) Gamelin, D. R.; Güdel, H. U. *Acc. Chem. Res.* **2000**, *33*, 235−242.
(14) Bussière, G.; Beaulac, R.; Cardinal-David, B.; Reber, C. *Coord. Chem. Rev.* **2001**, *219−221*, 509−543.
(15) Krzystek, J.; Fiedler, A. T.; Sokol, J. J.; Ozarowski, A.; Zvyagin, S. A.; Brunold, T. C.; Long, J. R.; Brunel, L.-C.; Telser, J. *Inorg. Chem.* **2004**, *43*, 5645−5658.
(16) Tregenna-Piggott, P. L. W.; Weihe, H.; Bendix, J.; Barra, A.-L.; Güdel, H.-U. *Inorg. Chem.* **1999**, *38*, 5928−5929.
(17) Tregenna-Piggott, P. L. W.; Best, S. P.; Güdel, H. U.; Weihe, H.; Wilson, C. C. *J. Solid State Chem.* **1999**, *145*, 460−470.

10.1021/ic051709f CCC: $33.50
Published on Web 03/24/2006

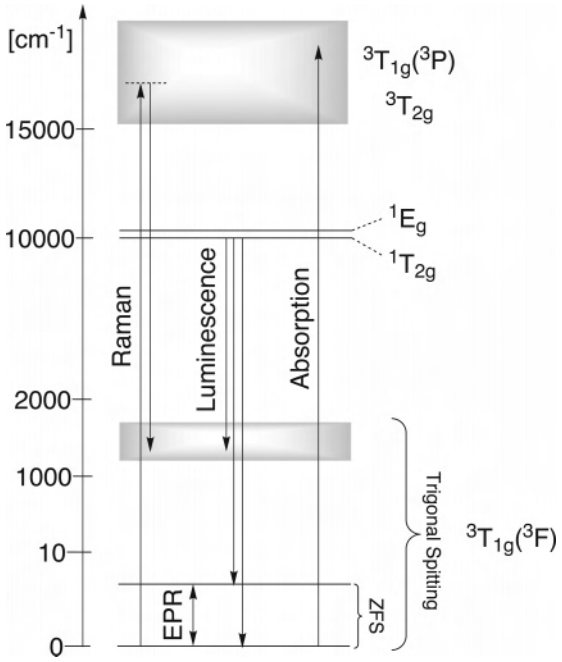

Figure 1. Schematic view of the electronic states of a trigonally distorted octahedral vanadium(III) complex with O_h symmetry labels. The different experimental transitions probed are shown as arrows. Note the nonlinear energy scale.

complexes, such as $[V(H_2O)_6]^{3+}$, for which new insight on the interplay between ligand coordination and the electronic structure of metal-centered states has been obtained.[16−18,22,23]

We report the spectroscopic characterization of the ground state and of the lowest-energy electronic excited states of $[V(urea)_6](ClO_4)_3$. This complex has been intensively studied over the past 50 years[11,25−32], but no direct measurement of the ground-state trigonal splitting, Δ, shown in Figure 1, has been reported. Ligand-field calculations reported a value of about 1300 cm^{-1},[30] but another study based on least-squares fits to the magnetic susceptibility of $[V(urea)_6]^{3+}$ suggested a far lower value of only 300 cm^{-1} for Δ.[32] In a previous report, we pointed out that the NIR luminescence spectrum of $[V(urea)_6]I_3$ shows a very weak and broad transition at an energy lower by about 1400 cm^{-1} than the highest-energy electronic origin,[33] close to the calculated splitting value of 1300 cm^{-1}. We present here the Raman spectroscopy, high-frequency and high-field electron paramagnetic resonance (HF-EPR) spectra, magnetic susceptibility measurements, and the full NIR luminescence spectra of $[V(urea)_6](ClO_4)_3$ and its deuterated analogue $[V(urea\text{-}d_4)_6](ClO_4)_3$. The combination of all these techniques, illustrated schematically in Figure 1, provides precise information on the magnitude of the trigonal and spin-orbit splittings of the $^3T_{1g}$ (O_h) ground state and insight on the origin of the large trigonal splitting in the title complex. A set of ligand-field parameters in the framework of the angular overlap model (AOM) that correctly describe all spectroscopic data reported here is also given.

2. Experimental Section

Complexes were prepared as described previously.[33,34] Deuterated urea-d_4 was obtained by dissolving urea in a minimum amount of warm D_2O and evaporating to dryness. The process was repeated five times, and the degree of deuteration was determined to be at least 95% by comparing the relative intensities of the N−H/N−D stretching bands in the Raman spectrum. $[V(urea)_6]I_3$ and $[V(urea)_6](ClO_4)_3$ both crystallize as green crystals in the space group $R\bar{3}c$ with the V^{3+} ion located on a site of D_3 symmetry in the crystal.[26,27] Steady-state luminescence measurements were performed using the UV lines (333.6−363.8 nm) of an Ar^+ laser in broadband mode (Spectra-Physics Stabilite 2017−06S). Emission was dispersed through a 0.5 m monochromator (Spex 500M) and detected with a Ge detector (ADC 403L) cooled to 77 K. Sample cooling was achieved with a He gas continuous flow cryostat (Oxford CF-1204). The spectra reported here were corrected to eliminate the voltage spikes typical for germanium detectors.[35] A Raman microscope (Renishaw System 3000)[14] was used to measure Raman spectra. Samples were cooled with a Linkam THMS 600 cryostat using liquid nitrogen. HF-EPR spectra were obtained at the Grenoble High Magnetic Field Laboratory. Excitation frequencies of 190, 230, 285, 345, and 380 GHz were generated from the harmonics of sources operating at 95 and 115 GHz in conjunction with a static field ranging from 0 to 12 T. Spectra were recorded at 5 and 30 K on powdered samples. The temperature dependence of the magnetic susceptibility was measured on powdered samples with a Quantum Design MPMS superconductive SQUID magnetometer operating at a field strength of 0.5 T and in the temperature range of 2−300 K. The magnetic field dependence of the magnetization was measured on the same magnetometer in the field range of 0−5.5 T at 2 K. All experimental results were corrected for diamagnetism of the constituent atoms using Pascal constants. Semiempirical molecular orbital calculations were made with Gaussian 98 at the AM1 level.[36]

3. Results

3.1. Raman Spectra. Figure 2 shows the 77 K Raman spectra of urea, $[V(urea)_6](ClO_4)_3$, urea-d_4, and $[V(urea\text{-}d_4)_6](ClO_4)_3$. The spectra of urea and urea-d_4 have been reported in detail.[37,38] A comprehensive list of all peaks observed for

(18) Tregenna-Piggott, P. L. W.; Spichiger, D.; Carver, G.; Frey, B.; Meier, R.; Weihe, H.; Cowan, J. A.; McIntyre, G. J.; Zahn, G.; Barra, A.-L. *Inorg. Chem.* **2004**, *43*, 8049−8060.
(19) Anthon, C.; Bendix, J.; Schäffer, C. E. *Inorg. Chem.* **2003**, *42*, 4088−4097.
(20) Benmelouka, M.; Messaoudi, S.; Furet, E.; Gautier, R.; Le Fur, E.; Pivan, J.-Y. *J. Phys. Chem. A* **2003**, *107*, 4122−4129.
(21) Kallies, B.; Meier, R. *Inorg. Chem.* **2001**, *40*, 3101−3112.
(22) Tregenna-Piggott, P. L. W.; Carver, G. *Inorg. Chem.* **2004**, *43*, 8061−8071.
(23) Carver, G.; Spichiger, D.; Tregenna-Piggott, P. L. W. *J. Chem. Phys.* **2005**, *122*, 124511.
(24) Rudowicz, C.; Yang, Z.-Y.; Yeung, Y.-Y.; Qin, J. *J. Phys. Chem. Solids* **2003**, *64*, 1419−1428.
(25) Hartmann, H.; Furlani, C. *Z. Phys. Chem.* **1956**, *9*, 162−173.
(26) Figgis, B. N.; Wadley, L. G. B. *J. Chem. Soc., Dalton Trans.* **1972**, 2182−2188.
(27) Dingle, R.; McCarthy, P. J.; Ballhausen, C. J. *J. Chem. Phys.* **1969**, *50*, 1957−1962.
(28) Flint, C. D.; Greenough, P. *Chem. Phys. Lett.* **1972**, *16*, 369−370.
(29) Carlin, R. L.; McElearney, J. N.; Schwartz, R. W.; Siegel, A. E. *J. Am. Chem. Soc.* **1971**, *93*, 4337−4338.
(30) Rahman, H. U. *J. Phys. C: Solid State Phys.* **1971**, *4*, 3301−3306.
(31) Baker, J.; Figgis, B. N. *Aust. J. Chem.* **1975**, *28*, 439−442.
(32) Baker, J.; Figgis, B. N. *Aust. J. Chem.* **1980**, *33*, 2377−2385.
(33) Beaulac, R.; Tremblay, J.-C.; Bussière, G.; Reber, C. *Can. J. Anal. Sci. Spectrosc.* **2001**, *46*, 152−161.
(34) Hartmann, H.; Schläfer, H. L.; Hansen, K. H. *Z. Anorg. Chem.* **1956**, *284*, 153−161.
(35) Oetliker, U.; Reber, C. *J. Near Infrared Spectrosc.* **1995**, *3*, 63−71.

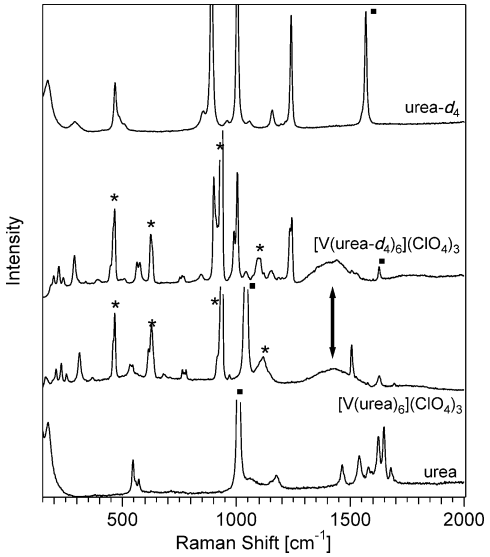

Figure 2. Solid-state Raman spectra of urea-d_4, $[V(urea\text{-}d_4)_6](ClO_4)_3$, $[V(urea)_6](ClO_4)_3$, and urea, at 77 K. Asterisks denote vibrations of the perchlorate anion. The vertical double arrow shows the electronic Raman transition. The small squares at approximately 1000 and 1600 cm^{-1} indicate peaks that shift significantly (approximately 50 cm^{-1}) upon deuteration.

urea-d_4 and $[V(urea\text{-}d_4)_6](ClO_4)_3$, as well as assignments of selected peaks are given in Table 1. The 100−500 cm^{-1} region in the spectra of $[V(urea)_6](ClO_4)_3$ and of $[V(urea\text{-}d_4)_6](ClO_4)_3$ is almost identical for both complexes, indicating very similar metal−ligand bonding. Most of the ligand-centered modes are found at the same frequencies in the spectra of the complexes as for uncoordinated urea. Some significant shifts are observed and discussed in detail below. The most important feature in the spectra of the vanadium(III) complexes is a broad band located at approximately 1430 cm^{-1}, indicated by the vertical arrow in Figure 2. This band, absent from the spectra of the uncoordinated ligands, is too broad and too high in energy to be a metal−ligand vibration and is assigned to an electronic Raman transition between two components of the electronic ground state. Such transitions are not uncommon in six-coordinated complexes of vanadium(III).[23,33,39−42] In contrast to peaks corresponding to vibrational transitions, the electronic band shows a significant decrease of intensity and becomes broader with increasing temperature for both $[V(urea)_6](ClO_4)_3$ and $[V(urea\text{-}d_4)_6](ClO_4)_3$.[33]

Table 1. Vibrational Frequencies (cm^{-1}) Determined from Raman Spectra and Assignments for Urea-d_4 and $[V(urea\text{-}d_4)_6](ClO_4)_3$

assignment[a]	urea-d_4	$[V(urea\text{-}d_4)_6](ClO_4)_3$
		198
		220
		240
		290
		340
		390
ν_2 $[ClO_4]^-$	459	448
δ (NCN)	470	466
δ (NCO)	512	510
		563, 576
ν_4 $[ClO_4]^-$	625	624
		761
	854	846
ND_2 rocking	892	901
ν_1 $[ClO_4]^-$	928	937
ν $(CN)_{sym}$	1004	990
		1004
		1043
ν_3 $[ClO_4]^-$	1119	1098
NH_2 rocking (traces)	1157	1154
ND_2 bending	1241	1235, 1244
ν (CO)	1569	1626
ν (ND)	2425, 2506, 2589	2457, 2501, 2629
ν (NH) (traces)	3392	3388, 3433, 3466

[a] Assignments for urea based on the normal-mode analysis in ref 37; frequencies for $[ClO_4]^-$ from ref 56, Vol. A, p 199, Table II-6e.

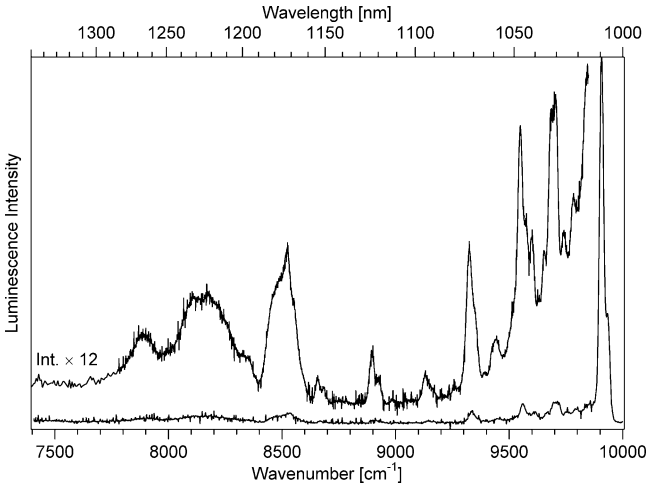

Figure 3. Luminescence spectrum of $[V(urea\text{-}d_4)_6](ClO_4)_3$ at 25 K.

3.2. Luminescence Spectra. The NIR luminescence spectrum of $[V(urea\text{-}d_4)_6](ClO_4)_3$ between 7500 and 10 000 cm^{-1} is presented in Figure 3. The most intense feature at all temperatures is the narrow peak located at 9907 cm^{-1}, which is easily assigned in the D_3 point group symmetry of the title complex as the $^1E(O_h{:}^1T_{2g}) \rightarrow {}^3A_2(O_h{:}^3T_{1g})$ intraconfigurational transition, as was first reported by Flint and Greenough.[28] The lowest-energy spin-flip transition is observed in the 9500−10 500 cm^{-1} energy range for many different vanadium(III) complexes.[14,28,33,43−46] The shoulder

(36) Frisch, M. J.; Trucks, G. W.; Schlegel, H. B.; Scuseria, G. E.; Robb, M. A.; Cheeseman, J. R.; Zakrzewski, V. G.; Montgomery, J. A., Jr.; Stratmann, R. E.; Burant, J. C.; Dapprich, S.; Millam, J. M.; Daniels, A. D.; Kudin, K. N.; Strain, M. C.; Farkas, O.; Tomasi, J.; Barone, V.; Cossi, M.; Cammi, R.; Mennucci, B.; Pomelli, C.; Adamo, C.; Clifford, S.; Ochterski, J.; Petersson, G. A.; Ayala, P. Y.; Cui, Q.; Morokuma, K.; Malick, D. K.; Rabuck, A. D.; Raghavachari, K.; Foresman, J. B.; Cioslowski, J.; Ortiz, J. V.; Baboul, A. G.; Stefanov, B. B.; Liu, G.; Liashenko, A.; Piskorz, P.; Komaromi, I.; Gomperts, R.; Martin, R. L.; Fox, D. J.; Keith, T.; Al-Laham, M. A.; Peng, C. Y.; Nanayakkara, A.; Challacombe, M.; Gill, P. M. W.; Johnson, B.; Chen, W.; Wong, M. W.; Andres, J. L.; Gonzalez, C.; Head-Gordon, M.; Replogle, E. S.; Pople, J. A. *Gaussian 98*, revision A.9; Gaussian, Inc.: Pittsburgh, PA, 1998.
(37) Yamaguchi, A.; Miyazawa, T.; Shimanouchi, T.; Mizuchima, S. *Spectrochim. Acta* **1957**, *10*, 170−178.
(38) Stewart, J. E. *J. Chem. Phys.* **1957**, *26*, 248−254.
(39) Best, S. P.; Clark, R. J. H. *Chem. Phys. Lett.* **1985**, *122*, 401−405.
(40) Spichiger, D.; Carver, G.; Dobe, C.; Bendix, J.; Tregenna-Piggott, P. L. W.; Meier, R.; Zahn, G. *Chem. Phys. Lett.* **2001**, *337*, 391−397.
(41) Tregenna-Piggott, P. L. W.; Best, S. P. *Inorg. Chem.* **1996**, *35*, 5730−5736.
(42) Berg, R. W.; Boghosian, S.; Bjerrum, N. J.; Fehrmann, R.; Krebs, B.; Sträter, N.; Mortensen, O. S.; Papatheodorou, G. N. *Inorg. Chem.* **1993**, *32*, 4714−4720.
(43) Champagnon, B.; Duval, E. *J. Physique Lett.* **1977**, *38*, 299−301.
(44) Goldschmidt, Z.; Low, W.; Foguel, M. *Phys. Lett.* **1965**, *19*, 17−18.
(45) Reber, C.; Güdel, H. U. *J. Lumin.* **1988**, *42*, 1−13.

Scheme 1

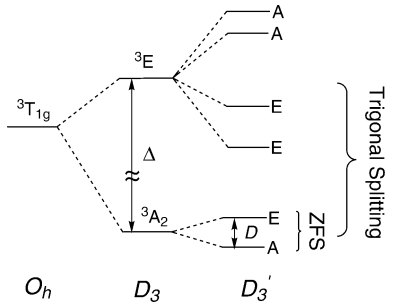

at 9932 cm^{-1} is a hot band and is thus assigned to a transition from a thermally populated state, located 25 cm^{-1} higher in energy than the ^{1}E (O_h·^{1}T$_{2g}$) emitting state. This is further confirmed by absorption spectroscopy which shows such a state at 9933 cm^{-1}.[27] Dingle et al.[27] were also able to resolve each of these two peaks into two components separated by approximately 5 cm^{-1}. This very small splitting was assigned to the zero-field splitting (ZFS, Figure 1 and Scheme 1) of the lowest-energy ground-state component, in agreement with the 5.8 cm^{-1} value estimated later by calorimetry by Carlin.[29] HF-EPR and magnetism studies of the complex also confirm this value, as discussed in the next sections.

In an earlier report, we presented the luminescence spectrum of nondeuterated [V(urea)$_6$]I$_3$.[33] A large, unresolved system of bands was observed in the luminescence spectrum of [V(urea)$_6$]I$_3$ at energies around 8500 cm^{-1}, but its overall intensity was weak and the signal-to-noise ratio very low. The higher quality of the corresponding region in the spectrum of the deuterated complex in Figure 3 is most likely the result of a reduction of the efficiency of nonradiative deactivation pathways; this suggests that modes involving N−H quanta act as efficient quenchers for the luminescence, even at very low temperatures. No shift in energy is observed for any of the peaks in the spectrum upon deuteration. A series of peaks lying at lower energy than the 9907 cm^{-1} electronic origin are now clearly distinguished. We divide those peaks into two apparently different types. The first type are narrow transitions between 8800 and 9900 cm^{-1} (i.e., lower in energy than the electronic origin by 100 to 1100 cm^{-1}). They are assigned as vibronic origins. Figure 3 shows that most of the emitted intensity is located in the electronic origin transition at 9907 cm^{-1}. [V(urea)$_6$]$^{3+}$ does not have a center of inversion, and as a result, only a small proportion of the overall intensity is observed as vibronic in origin, in contrast to complexes with inversion symmetry, where vibronic origins dominate.[45,47] The second type of transition observed includes broader, unresolved bands located at lower energy, between 7800 and 8600 cm^{-1}. Comparison with the Raman results presented above suggests that these bands correspond to an electronic transition between ^{1}E(O_h·^{1}T$_{2g}$) and the ^{3}E component of the ground state, located higher in energy by approximately 1400 cm^{-1} than the ^{3}A$_2$ component, as illustrated in Scheme 1.

(46) Riseberg, L. A.; Moos, H. W.; Partlow, W. D. *IEEE J. Quantum Electron.* **1968**, *QE-4*, 609−612.
(47) Reber, C.; Güdel, H. U. *Chem. Phys. Lett.* **1989**, *154*, 425−431.

Table 2. Resonant Field Positions for HF-EPR Data Obtained for [V(urea)$_6$](ClO$_4$)$_3$ at 5 K and Spin Hamiltonian Parameters Derived from a Least-Squares Fit to the Observed Data

frequency (GHz)	obsd field (G)	calcd field (G)	difference obsd − calcd
189.9982	90 221	90 596	−375
189.9982	114 970	114 946	23
229.9988	32 074	31 706	367
229.9988	51 543	51 585	−42
229.9988	107 320	107 179	141
344.9982	51 085	51 688	−603
344.9982	83 698	83 611	87
344.9982	101 450	101 699	−249
379.9964	73 272	73 217	55
379.9964	98 063	98 076	−13
379.9964	116 142	116 041	101

param	value
g_x	1.848(2)
g_y	1.832(4)
g_z	1.946(7)
D	6.00(2) cm^{-1}
E	0.573(6) cm^{-1}

3.3. HF-EPR. Vanadium(III) ions, as other integer-spins ions, are typically "silent" to conventional EPR spectroscopy. This effect, inherent to non-Kramers ions, is particularly important for vanadium(III) systems because of their large ground-state zero-field splitting. High-field multifrequency EPR techniques (HF-EPR)[48,49] have enabled the study of the ground-state of vanadium(III) complexes.[15−18] HF-EPR measurements have been conducted on a powdered sample of [V(urea)$_6$](ClO$_4$)$_3$, and a total of 17 resonances were observed. Since no resonance showed hyperfine resolution, coupling of the electron spin to the nuclear spin of the vanadium center was neglected in the analysis. A conventional spin Hamiltonian (eq 1), using $S = 1$, was used to interpret all EPR spectra.[50] The calculated field positions

$$\hat{H} = g_z\mu_B B_z\hat{S}_z + g_y\mu_B B_y\hat{S}_y + g_x\mu_B B_x\hat{S}_x + D\left[\hat{S}_z^2 - \frac{1}{3}S(S+1)\right] + E[\hat{S}_x^2 - \hat{S}_y^2] \quad (1)$$

were obtained by least-squares fits of the parameters in eq 1 to the observed data with the EPR simulation program SIM.[51,52] Accurate values of the spin Hamiltonian parameters were obtained by minimizing

$$\chi^2 = \sum_i \frac{(B_{\mathrm{obsd},i} - B_{\mathrm{calcd},i})^2}{\sigma_i^2} \quad (2)$$

where i runs over 11 observed resonance magnetic fields, $B_{\mathrm{obsd},i}$, and $B_{\mathrm{calcd},i}$ and σ are the calculated resonance magnetic field and an uncertainty associated with the ith observation, respectively. The latter was chosen as a third of the

(48) Riedi, P. C.; Smith, G. M. *Electron Paramagn. Reson.* **2004**, *19*, 338−373.
(49) Smith, G. M.; Riedi, P. C. *Electron Paramagn. Reson.* **2000**, *17*, 164−204.
(50) Abragam, A.; Bleaney, B. *Electron Paramagnetic Resonance of Transition Metal Ions;* Oxford University Press: Oxford, U.K., 1970.
(51) Glerup, J.; Weihe, H. *Acta Chem. Scand.* **1991**, *45*, 444−448.
(52) Jacobsen, C. J. H.; Pedersen, E.; Villadsen, J.; Weihe, H. *Inorg. Chem.* **1993**, *32*, 1216−1221.

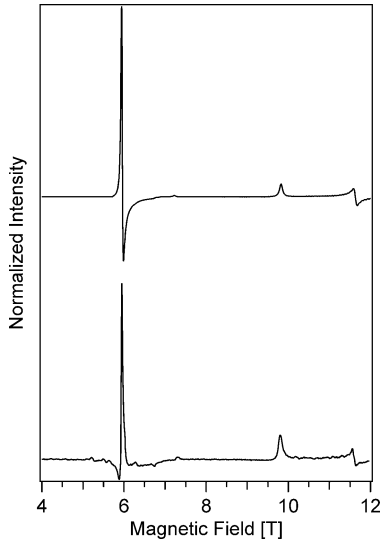

Figure 4. (bottom) Experimental powder HF-EPR spectrum of $[V(urea)_6](ClO_4)_3$ at 5 K and a probe frequency of 380 GHz. (top) Simulated spectrum using the spin Hamiltonian described in the text (eq 1) and the parameters listed in Table 2.

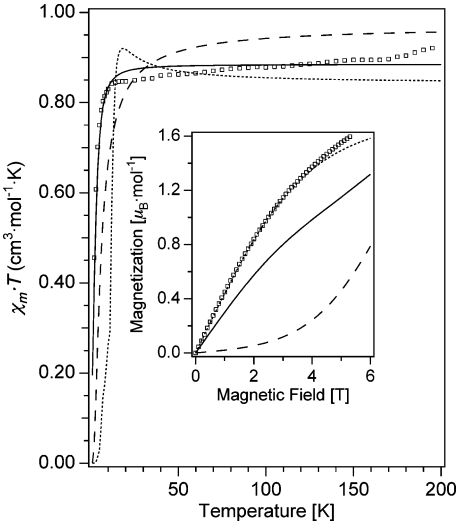

Figure 5. Temperature dependence of $\chi_M T$ for powdered $[V(urea)_6](ClO_4)$: □, experimental; —, theoretical curve for $\chi_M T_{(av)}$; · · · and - - -, theoretical curves for $\chi_M T_{(x)}$ and $\chi_M T_{(z)}$, respectively. The inset shows the magnetic field dependence of the magnetization at 2 K for $[V(urea)_6](ClO_4)_3$, using the same symbols as in the main figure.

experimental bandwidth. The resulting parameter values are listed in Table 2. A typical experimental HF-EPR spectrum is shown in Figure 4, along with the corresponding simulation; the spin Hamiltonian parameters derived from this analysis are given in Table 2. A slight deviation from axial symmetry ($g_x \neq g_y$ and $E \neq 0$) appears to be present at 5 K; the deviation from perfect D_3 symmetry is very small and negligible for the analysis of other aspects of the electronic structure such as the ground-state trigonal splitting in section 4.2. The zero-field splitting determined from analysis of the EPR spectra is in agreement with the literature[27,29] and the magnetic measurements discussed in the next section.

3.4. Magnetic Measurements. The variation of χT of $[V(urea)_6](ClO_4)_3$ is given as a function of temperature in Figure 5 and is in very good agreement with previous reports (see Supporting Information).[11,32] The room-temperature value of χT is slightly below 0.99 cm^3 mol^{-1} K and decreases slowly with decreasing temperature down to approximately 50 K. Below 50 K, χT drops quickly and reaches 0.46 cm^3 mol^{-1} K at 2 K. This decrease at very low temperatures is expected for a trigonally split $^3T_{1g}$ (O_h) state having its $^3A_2$ component at lower energy and subjected to spin−orbit coupling; the zero-field splitting of the $^3A_2$ state is given by the parameter D determined by EPR and illustrated in Scheme 1. Given the large trigonal splitting, Δ, of the $^3T_{1g}$ (O_h) state experimentally determined in sections 3.1 and 3.2, only the spin−orbit components of the $^3A_2$ state (D_3 symmetry) are expected to be significantly populated and they dominate the magnetic susceptibility. The lowest level of $^3A_2$ is a nondegenerate A state, as shown in Scheme 1, and the susceptibility is expected to drop as the temperature decreases and the higher-energy E component of $^3A_2$ is depopulated. The magnetization of the complex at variable magnetic fields is shown in the inset to Figure 5. The magnetization appears to increase approximately linearly with the applied magnetic field up to 2 T. At higher fields, the magnetization increases less rapidly but does not seem to reach a plateau even at 5.5 T. The same $S = 1$ spin Hamiltonian (eq 1) described in the previous section (but neglecting the small rhombic distortion E) and the parameter values given in Table 2 have been used to simulate the theoretical magnetic behavior of $[V(urea)_6](ClO_4)_3$, using the following equations[53]

$$M = \frac{N\sum_n \left(-\frac{\partial E_n}{\partial B}\right)\exp\left(-\frac{E_n}{kT}\right)}{\sum_n \exp\left(-\frac{E_n}{kT}\right)} \quad (3)$$

$$\chi = \frac{\partial M}{\partial B} \quad (4)$$

where M is the molar magnetization, χ the molar magnetic susceptibility, B the applied magnetic field, T the temperature, and the E_n respresents the eigenvalues of the spin-Hamiltonian. N and k are Avogadro's and Boltzmann's constants, respectively. The simulations are given in Figure 5 for an applied field in the x,y direction ($\chi T_{(x)}$, $M_{(x)}$), along the z axis ($\chi T_{(z)}$, $M_{(z)}$), and also for an average field direction ($\chi T_{(av)}$, $M_{(av)}$) approximated by[53]

$$\chi_{(av)} = \frac{2\chi_{(x)} + \chi_{(z)}}{3} \quad (5)$$

The quick increase of χT and the plateau follow the calculated $\chi_{(av)}$ curve quite well, especially in view of the absence of any adjustable parameters. At temperatures higher than 50 K, the experimental value of χT increases steadily, whereas the theoretical curve stays constant at about 0.90 cm^3 mol^{-1} K. The magnetization of the sample follows the perpendicular-field simulation curve quite well, suggesting

(53) Kahn, O. *Molecular Magnetism;* Wiley-VCH: New York, 1993; p 17.

Scheme 2

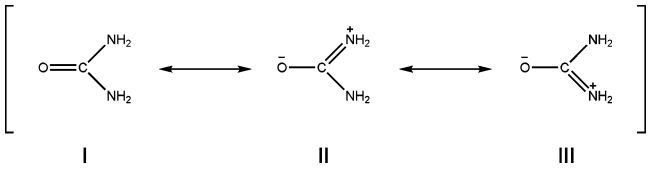

I II III

that the molecular C_3 axes of the complexes in the sample are aligned perpendicularly to the strong magnetic field. Because of the weak field used for the measurements of χT (0.5 T), any effect of alignment is expected to be negligible. It is likely that small temperature-dependent structural changes lead to the increase of χT with temperature to a value close to the spin-only value of 0.994 $cm^3\ mol^{-1}\ K$ at room temperature. The low-temperature magnetic experiments can be well characterized from the energy levels shown in Scheme 1 and quantitatively rationalized with the parameters from the spectroscopic studies discussed above.

4. Discussion

4.1. Coordination of Urea Ligands to the Metal Center. Urea ligands can coordinate to a metal center either by the oxygen or by one of the nitrogen atoms.[54] In the case of $[V(urea)_6]^{3+}$, X-ray diffraction results show that coordination occurs via the oxygen atom of urea.[26] Past structural studies on urea have suggested that the electronic structure of uncoordinated urea is best described by a resonance hybrid of the three structures, I, II, and III, shown in Scheme 2, with contributions of 40, 30, and 30%, respectively, from each resonance structure.[55] This has led Nakamoto[56] and others[57,54] to argue that structures II and III should prevail in complexes of oxygen-coordinated urea, thus predicting a decrease of the C═O stretching frequency upon coordination. Previous studies reported such decreases in infrared spectra for complexes of chromium(III)[54] and scandium(III).[54,57] One problem with this approach is the difficulty to unambiguously assign the actual frequency for the pure C═O stretching mode in uncoordinated urea since this group vibration mixes strongly with C−N stretching, mainly because of the similar masses of the oxygen atom and the NH_2 group.[37] The C═O stretching region (1450−1750 cm^{-1}) in the Raman spectrum of free urea (Figure 2) shows at least six peaks all located within a range of 250 cm^{-1}. Any determination of the main C═O stretching frequency and of shifts with metal coordination is somewhat ambiguous. A more direct way to probe the change in the electronic structure of the ligand upon coordination to the metal is based on a comparison of the bond lengths of coordinated and free urea. In the case of $[V(urea)_6]I_3$, a shortening of the C═O bond of urea is clearly observed in the complex. The bond length of C═O in free urea is 1.258 Å;[58] it decreases to 1.17(1) Å in $[V(urea)_6]I_3$,[26] clearly showing that coordinated urea has a different structure than its free form. This change modifies the electronic structure of the ligand, making any analysis based on the structure of the free ligand inadequate to predict or explain the spectroscopic observations.

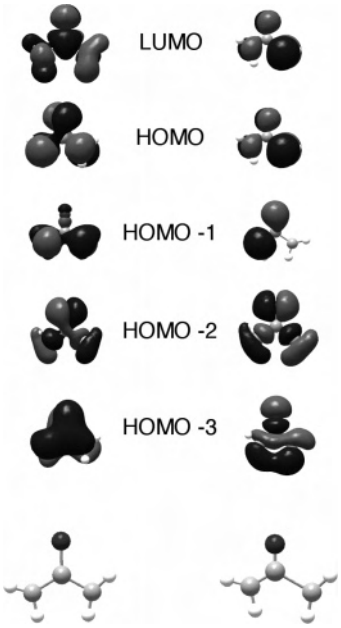

Figure 6. Molecular orbitals for urea in its uncoordinated form (left) and in the structure it adopts in $[V(urea)_6]^{3+}$ (right). Schematic structures are shown at the bottom; the distortions of the structure on the right have been amplified to clearly illustrate the differences from the left-hand structure.

The vibrational spectra of free and vanadium(III)-coordinated urea ligands in Figure 2 support the idea that the C═O bond becomes stronger with coordination. Deuteration of urea reduces the mixing between C−N and C═O stretching,[37] resulting in the simpler Raman spectrum of urea-d_4 in the 1250−1750 cm^{-1} region. In this case, there is a clear increase (57 cm^{-1}) of the C═O stretching frequency between urea-d_4 and $[V(urea\text{-}d_4)_6](ClO_4)_3$, indicated by the peaks labeled with black squares in the Raman spectra in Figure 2. The case of the nondeuterated ligand and its vanadium complex is less obvious. Outside the 1500−1750 cm^{-1} region, a shift of the strong 1010 cm^{-1} peak in urea to 1046 cm^{-1} in $[V(urea)_6](ClO_4)_3$ is unambiguously seen in the Raman spectra in Figure 2. A normal coordinate analysis of urea assigned this mode to a C−N stretch with substantial contributions from the C═O stretch;[37] it is likely that this C═O contribution is responsible for the increase in frequency observed in the spectrum of $[V(urea)_6](ClO_4)_3$, another confirmation of the stronger C═O bond in the complex. An adequate description of the bonding between urea and vanadium(III) involves the structure of the ligand, its molecular orbitals and their interaction with the orbitals of the metal center.

A qualitative representation of the relevant molecular orbitals of uncoordinated urea is given in Figure 6. The most stable calculated geometry at the AM1 level has C_2 point-group symmetry, where the N−H bonds are almost in the

(54) Penland, R. B.; Mizushima, S.; Curran, C.; Quagliano, J. V. *J. Am. Chem. Soc.* **1957**, *79*, 1575−1578.
(55) Vaughan, P.; Donohue, J. *Acta Crystallogr.* **1952**, *5*, 530−535.
(56) Nakamoto, K. *Infrared and Raman Spectra of Inorganic and Coordination Compounds*; John Wiley & Sons: New York, 1997; Vol. B, p 100.
(57) Firsova, N. L.; Kolodyazhnyi, Y. V.; Osipov, O. A. *J. Gen. Chem. USSR (Engl. Transl.)* **1969**, *39*, 2101−2104.
(58) Zavodnik, V.; Stash, A.; Tsirelson, V.; de Vries, R.; Feil, D. *Acta Crystallogr.* **1999**, *B55*, 45−54.

molecular plane. The same geometry was recently obtained with different electronic structure calculations.[59] X-ray diffraction studies of urea show that the C−N bonds are equivalent.[58] Coordination to vanadium(III) removes this equivalency, as assessed by the net difference of the C−N bond lengths measured crystallographically (C−N bond lengths at 90 K are 1.39 and 1.23 Å).[26] Furthermore, as discussed above, the C═O bond is shorter in the coordinated form. The cause for these significant changes in the structure of urea can be separated into two different contributions: (1) interaction with neighboring molecules and (2) bonding to the metal center. Hydrogen bonds are expected to be the main intermolecular interactions for urea. Since the packing of molecules in the crystal is very different in pure urea than in $[V(urea)_6]^{3+}$, such interactions could force the observed change of structure. While hydrogen bonding undoubtedly plays a major role in stabilizing the complex and in favoring the tilting of urea,[26] it cannot solely account for the structural changes of urea. We note that the same frequency is observed within experimental precision for the C═O stretching mode in both the deuterated and nondeuterated complexes, suggesting that deuteration does not influence the C═O bond, which then implies that metal−ligand bonding is the main cause for the shortening of the C═O bond. Furthermore, the electronic structure of the ground state of $[V(urea)_6](ClO_4)_3$, $[V(urea\text{-}d_4)_6](ClO_4)_3$, and $[V(urea)_6]I_3$, as probed by NIR luminescence spectroscopy, does not differ despite deuteration and the counterion substitution. These observations show that metal−ligand bonding plays a dominant role in changing the structure of the ligand. At least some of the ligand deformation, in particular the C═O bond shortening, is caused by the interaction with the metal center. A likely description of the structure of coordinated urea would include contributions of resonance structure I to explain the C═O bond shortening and resonance structure II, leading to the significantly different C−N bond lengths. The key aspects in understanding this are why these structural changes occur and how they contribute to the split of the electronic ground state of $[V(urea)_6]^{3+}$. Figure 6 compares the molecular orbitals of uncoordinated urea with those of a urea molecule with the structure of the coordinated ligand. Both the shapes of the molecular orbitals and their energies change, as given in the Supporting Information. The most important difference shown in Figure 6 is the fact that the distorted ligand has a set of orbitals much more adapted to maximize π-interactions with the metal because they are either perfectly perpendicular to the molecular plane or exactly within the plane. In contrast, the orbitals of uncoordinated urea lack this alignment; for example, the HOMO and HOMO-2 orbitals are mainly oxygen p orbitals, but they are not perpendicular to the molecular plane; furthermore, there are no π-donating orbitals located in the molecular plane. We therefore conclude that the change of structure of urea enables it to coordinate more efficiently to the metal and that this energetic stabilization more than compensates the destabilization of the distorted structure. It is likely that π-interactions are mainly responsible for this stabilization.

(59) Godfrey, P. D.; Brown, R. D.; Hunter, A. N. *J. Mol. Struct.* **1997**, *413−414*, 404−414.

Table 3. AOM Parameters for $[V(urea)_6]^{3+}$

param	value (cm^{-1})	Euler angles[a]	value (deg)[b]
e_σ	6101	Θ_1, Φ_1, Ψ_1	54.38, 0.0, 25.0
$e_{\pi\|\|}$	875	Θ_2, Φ_2, Ψ_2	54.38, 120.0, 25.0
$e_{\pi\perp}$	0	Θ_3, Φ_3, Ψ_3	54.38, 240.0, 25.0
B	632	Θ_4, Φ_4, Ψ_4	125.62, 187.0, −25.0
C	2877	Θ_5, Φ_5, Ψ_5	125.62, 307.0, −25.0
ζ	166	Θ_6, Φ_6, Ψ_6	125.62, 67.0, −25.0

[a] Perfect octahedron: $\Theta = 54.7°, \Phi = 125.3°$. [b] Θ and Φ angles taken from ref 26; Ψ angles calculated as described in section 4.2.

Urea binds to the metal with a V−O−C angle of 137° at room temperature (133° at 90 K).[26] The V−O−C fragments are expected to be bent because of the hydrogen bonding between adjacent ligands and because of different π-interactions parallel and perpendicular to the plane of the ligand. This deviation from orthoaxial symmetry (i.e., the urea ligand no longer has C_{2v} pseudo-symmetry with respect to the metal−ligand axis) makes a big contribution to the strong trigonal distortion probed here by spectroscopic techniques. The VO_6 skeleton shows only a small deviation from perfectly octahedral coordination geometry by less than one degree in terms of compression of the octahedron along the C_3 axis, as given in Table 3 and by about 7° in terms of the twist of the two sets of three oxygen atoms related through the trigonal axis. As discussed in the next section, anisotropy of the metal−ligand π-bonds is the dominant contribution to the trigonal splitting in urea complexes. This situation is also encountered in other d^2 transition metal complexes.[15,17,18,33,39]

4.2. Ground-State Electronic Structure. The ground state electronic structure of six-coordinated vanadium(III) complexes depends on the nature and arrangement of the ligands. The simplest cases occur for monatomic ligands with perfectly octahedral coordination geometry: in this situation, spin-orbit coupling splits the $^3T_{1g}$ ground state into three components, each of which transforms the same way as those arising from the free-ion $^3P_{2,1,0}$ terms. This situation is encountered in vanadium(III)-doped Cs_2NaYCl_6 elpasolite crystals.[45] It appears, however, that in most complexes with molecular ligands the point-group symmetry at the vanadium(III) center is lower, leading to different splitting patterns. As a result of the trigonal field in the title complex, the $^3T_{1g}$ (O_h) ground state separates into two components, as shown in Scheme 1, with each component being further separated by spin-orbit coupling. The spectroscopic results presented above allow us to experimentally determine these energy spacings.

One of the most important features of the Raman and luminescence spectra in Figures 2 and 3 is the broad band corresponding to the transition to the higher-energy ^3E (D_3) ground-state component. The ground-state splitting allows a direct evaluation of the energetic consequences of the structural deviations from perfect octahedral geometry and is also a very sensitive probe of the bonding of the ligands to the metal center. For $[V(urea)_6]^{3+}$, this splitting is on the

order of 1400 cm^{-1}, and the spacing of the four spin−orbit components of ^3E is approximately 130 cm^{-1}. Neither the Raman nor the luminescence spectra show enough resolution to exactly measure the energy of each of these components. A somewhat higher resolution was found for the $^3A_g \rightarrow {}^3E_g$ (S_6) electronic Raman transition in $Rb[V(H_2O)_6](SO_4)_2 \cdot 6H_2O$,[41] and a pronounced reduction of the bandwidth was observed upon deuteration of the ligands. It has been suggested that the profile of the electronic Raman band was probably dominated by intensity-enhanced overtones of Jahn-Teller active vibrations.[22] The electronic Raman band of $[V(urea)_6]^{3+}$ does not show any apparent change of position and width with deuteration of the ligand, in contrast to that of $[V(H_2O)_6]^{3+}$, suggesting that the vibrational modes acting as vibronic origins are devoid of N−H (N−D) character.

We use a simple model for the urea ligands in the framework of the angular overlap model (AOM)[60−64] to analyze the spectroscopic features of the ground state. The main advantage of the AOM formalism is the ease with which it can reproduce the splitting of d−d states for any point-group symmetry.[64] Moreover, in contrast to conventional ligand field calculations, AOM parameters can be, up to a certain extent, transferred between similar systems.[65] In the simple model used here, six parameters are defined. Three of these describe the overlap between vanadium(III) and urea orbitals: e_σ is a sum of all the σ contributions to the overall metal−ligand overlap, $e_{\pi\perp}$ and $e_{\pi||}$ define out-of-plane and in-plane π-contributions, respectively. The three remaining parameters are Racah's electron−electron repulsion parameters B and C, and the spin−orbit coupling constant ζ. The free-ion values of these three parameters for vanadium(III) are $B_0 = 861$ cm^{-1}, $C_0 = 3815$ cm^{-1},[66] and $\zeta_0 = 206$ cm^{-1}.[67] These parameters become smaller with covalent metal−ligand bonding, mainly because of the nephelauxetic effect.[68,69] In addition to these six parameters, a set of three Euler angles for each ligand i is required: Θ_i, Φ_i, and Ψ_i give the angular geometry of the complex, with the quantization axis coincident with the 3-fold axis, as defined by Schäffer.[17,62,70] The first two of these angles are readily available from crystallography[26] and are listed in Table 3, along with all other AOM quantities. The third angle, Ψ_i, defines the orientation of the π system of the ligand in relation to that of the metal. The case of urea is slightly more complex than that of linear ligands, because urea binds to the metal with a V−O−C angle of about 135°, leading to bent bonding.[71] This generally leads to the so-called misdirected valency effect, a mix of σ- and π-interactions between the orbitals of the metal and the ligand, described in the AOM framework by an additional parameter $e_{\sigma\pi}$.[64,71] We do not include this effect in our analysis for two reasons. First, the traditional angular overlap model reproduces all spectroscopic features well and any additional parameter could lead to overparametrization of the system. Second, DFT calculations on an analogous complex, $[Cr(urea)_6]^{3+}$ (Supporting Information), show that the distribution of electronic density between the metal and the urea ligands has approximate cylindrical symmetry around the metal-ligand bond, suggesting that the extent of misdirected valency may not be as important as expected from the nonlinear V−O−C geometry. The angle Ψ for each ligand was thus calculated from the crystallographic data[26] as the angle between the vector normal to the plane defined by the quantization axis (molecular C_3 axis) and the V−O bond vector and the plane which contains the V−O bond vector and is parallel to the N−N bond vector, as illustrated elsewhere.[17] Since only the difference between $e_{\pi\perp}$ and $e_{\pi||}$ defines the effects of anisotropic π-bonding, the value of the smaller e_π parameter, which was found to be $e_{\pi\perp}$, was set to 0.[18]

Table 4. Observed and Calculated Energies of Electronic States of $[V(urea)_6]^{3+}$ Using the AOM Parameters in Table 3

state			calcd energy (cm^{-1})	obsd energy (cm^{-1})
O_h	D_3	D_3'		
$^3T_{1g}$ (^3F)	$^3A_2$	A	0	0
		E	6	6[a]
	^3E	E	1384	1400[b]
		E	1500	
		A	1601	
		A	1615	
$^1T_{2g}$	^1E	E	9907	9907[c]
	^1A	A	11 500	
^1E	^1E	E	11 675	
$^3T_{2g}$	$^3A_1$		15 534[d]	15 532[e]
	^3E		16 256[d]	16 518[e]
$^3T_{1g}$ (^3P)	$^3A_2$		23 668[d]	24 740[e]
	^3E		24 673[d]	

[a] HF-EPR, Figure 4. [b] Electronic Raman and luminescence, Figures 2 and 3. [c] Luminescence, Figure 3. [d] Calculated with parameters in Table 3, $\zeta = 0$. [e] Polarized absorption, ref 27.

Table 4 compares calculated energies using the AOM parameters listed in Table 3 with the experimental transition energies. The energies of the excited triplet states, observed by Dingle et al.,[27] are well reproduced by the set of parameters given in Table 3. The zero-field splitting, D, is equally well reproduced by the model. The spacing between the four spin-orbit components of ^3E is calculated to be about 200 cm^{-1}, in good agreement with the observed width of the electronic Raman band observed at approximately 1400 cm^{-1} in Figure 2 and with the luminescence band centered at 8500 cm^{-1} in Figure 3. The calculated trigonal splitting of the ground state (Δ in Scheme 1) is approximately 1500 cm^{-1}, in good agreement with the Raman and luminescence spectra. This large energy difference cannot be reproduced

(60) Jorgensen, C. K.; Pappalardo, R.; Schmidtke, H.-H. *J. Chem. Phys.* **1963**, *39*, 1422−1430.
(61) Larsen, E.; La Mar, G. N. *J. Chem. Educ.* **1974**, *51*, 633−640.
(62) Schäffer, C. E. *Struct. Bond.* **1968**, *5*, 68−95.
(63) Schäffer, C. E.; Jorgensen, C. K. *Mol. Phys.* **1965**, *9*, 401−412.
(64) Schönherr, T.; Atanasov, M. A.; Adamsky, H. Angular Overlap Model. In *Comprehensive Coordination Chemistry II*; McCleverty, J. A., Meyer, T. J., Eds.; Elsevier: Oxford, U.K., 2004; Vol. 2, p 443−455.
(65) Hoggard, P. E. *Struct. Bond.* **2004**, *106*, 37−57.
(66) Tanabe, Y.; Sugano, S. *J. Phys. Soc. Jpn.* **1954**, *9*, 766−779.
(67) Bendix, J.; Brorson, M.; Schäffer, C. E. *Inorg. Chem.* **1993**, *32*, 2838−2849.
(68) Jorgensen, C. K. *Prog. Inorg. Chem.* **1962**, *4*, 73−124.
(69) Schmidtke, H.-H. *Struct. Bond.* **2004**, *106*, 19−35.
(70) Adamsky, H.; Schönherr, T.; Atanasov, M. A. AOMX: Angular Overlap Model Computation. In *Comprehensive Coordination Chemistry II*; McCleverty, J. A., Meyer, T. J., Eds.; Elsevier: Oxford, U.K., 2004; Vol. 2, p 661−664.
(71) Bridgeman, A. J.; Gerloch, M. *Prog. Inorg. Chem.* **1997**, *45*, 179−281.

in the model without including π-anisotropy (i.e., $e_{\pi\perp} \neq e_{\pi||}$), indicating that this effect dominates the influence of deviations from octohedral symmetry of the ligator atom positions. The nature of the other broad bands between 7800 and 8400 cm^{-1} in the luminescence spectrum in Figure 3 is uncertain, as they are too low in energy to to correspond to components of ^3E. Their intensity is quite high for vibronic origins, especially in comparison to the striking difference in intensity of the vibronic origins built on the $^1E \rightarrow {}^3A_2$ transition seen in Figure 3. The calculated energy of the emitting singlet is in fair agreement with the experimental value. The parameters reported here for $[V(urea)_6]^{3+}$ compare well with those previously reported for $[V(H_2O)_6]^{3+}$.[17,18] The C/B ratio and ζ for the two complexes are the same ($C/B = 4.6$, $\zeta = 166$ cm^{-1}). The e_σ parameter for $[V(H_2O)_6]^{3+}$ ($e_\sigma = 6950$ cm^{-1}) is larger by 14% than that calculated for $[V(urea)_6]^{3+}$. The trigonal splitting for $[V(H_2O)_6]^{3+}$ (about 2000 cm^{-1})[17] is experimentally found to be larger than that for $[V(urea)_6]^{3+}$, in part because of the π-anisotropy for $[V(H_2O)_6]^{3+}$, where the difference between $e_{\pi||}$ and $e_{\pi\perp}$ of 930 cm^{-1} [17] is larger by 6% than for the title complex. In contrast to the water ligands, urea has significant π-bonding with metal-centered d orbitals both in the plane and perpendicular to the plane of the ligand, as illustrated by the molecular orbitals in the righthand column of Figure 6. The different Ψ angles for the two complexes also contribute to the observed trigonal splitting.

In summary, the components of the $^3T_{1g}$ (O_h) ground state have been characterized in detail for $[V(urea)_6]^{3+}$. Because of the high degeneracy of $^3T_{1g}$, many electronic states are found between 0 and 1500 cm^{-1}. The main perturbation is the trigonal field, leading to a trigonal splitting of approximately 1400 cm^{-1}. The trigonal field is mostly caused by the anisotropy of π-bonding. The importance of combining different experimental techniques to probe the ground state of vanadium(III) complexes is illustrated by this investigation.

Acknowledgment. Financial support from the Natural Sciences and Engineering Research Council (Canada) and the Fonds Québécois de la Recherche sur la Nature et les Technologies is acknowledged. We thank Thierry Lecomte-Poitras for help in measuring Raman and luminescence spectra. We also thank the Centre de Coopération Interuniversitaire France−Québec for a travel award to R.B.

Supporting Information Available: HF-EPR spectra, comparison of magnetic measurements with literature data (χT vs T), outputs of the semiempirical molecular orbital calculation of urea, of AOM calculations, and of simulations of the HF-EPR spectra (SIM program), and plots of some of the molecular orbitals of $[Cr(urea)_6]^{3+}$. This material is available free of charge via the Internet at http://pubs.acs.org.

IC051709F